Available online at www.sciencedirect.com
SCIENCE DIRECT®
Advances in Space Research 35 (2005) 214–222
ADVANCES IN SPACE RESEARCH (a COSPAR publication)
www.elsevier.com/locate/asr

The FLUKA code: New developments and application to 1 GeV/n iron beams

H. Aiginger [i], V. Andersen [d], F. Ballarini [c], G. Battistoni [b], M. Campanella [b], M. Carboni [k], F. Cerutti [b], A. Empl [d], W. Enghardt [h], A. Fassò [e], A. Ferrari [a,*,1], E. Gadioli [b], M.V. Garzelli [b,d], K. Lee [d], A. Ottolenghi [c], K. Parodi [h], M. Pelliccioni [k], L. Pinsky [d], J. Ranft [f], S. Roesler [a], P.R. Sala [b], D. Scannicchio [c], G. Smirnov [g], F. Sommerer [h,i], T. Wilson [j], N. Zapp [j]

[a] *CERN, CH-1211 Geneva, Switzerland*
[b] *University of Milan and INFN, Italy*
[c] *University of Pavia and INFN, Italy*
[d] *Houston University, Texas, USA*
[e] *SLAC, Stanford, USA*
[f] *Siegen University, Germany*
[g] *JINR, Dubna, Russia*
[h] *Forschungszentrum Rossendorf, Dresden, Germany*
[i] *Vienna University of Technology, Austria*
[j] *NASA/JSC, USA*
[k] *Laboratori Nazionali di Frascati, INFN, Italy*

Received 23 September 2004; received in revised form 28 January 2005; accepted 28 January 2005

Abstract

The modeling of ion transport and interactions in matter is a subject of growing interest, driven by the continuous increase of possible application fields. These include hadron therapy, dosimetry, and space missions, but there are also several issues involving fundamental research, accelerator physics, and cosmic ray physics, where a reliable description of heavy ion induced cascades is important.

In the present work, the capabilities of the FLUKA code for ion beams will be briefly recalled and some recent developments presented. Applications of the code to the simulation of therapeutic carbon, nitrogen and oxygen ion beams, and of iron beams, which are of direct interest for space mission related experiments, will be also presented together with interesting consideration relative to the evaluation of dosimetric quantities. Both applications involve ion beams in the *A*GeV range.

Keywords: Monte Carlo simulations; Heavy ion interactions; Therapeutic beams; Space dosimetry

1. Introduction

One of the important concerns about long term missions of astronauts, especially in deep space (such as in the case of a possible mission to Mars), is the biological risk from radiation. The effective dose per day due to galactic cosmic rays is ≈1 mSv, the order of magnitude

* Corresponding author.
E-mail address: alfredo.ferrari@cern.ch (A. Ferrari).
[1] On leave from INFN Milan.

0273-1177/$30 © 2005 Published by Elsevier Ltd on behalf of COSPAR.
doi:10.1016/j.asr.2005.01.090

of the dose on the Earth in one year. Moreover, one must take into account the risk of solar particle events, which are very intensive and unpredictable fluxes of particles (mainly protons) lasting up to few days, that in absence of appropriate shielding may determine a dose of several Sieverts.

Estimating biological risk from GCR and planning countermeasures are difficult tasks for several reasons: (a) it is necessary to have a detailed description of the effects of the spacecraft (and possible shields and shelters) in modulating the radiation fields; (b) the spectrum of the GCR, peaked at an energy of ≈1 GeV/n, has a significant presence of HZE particles, which represent only 1% of the particle flux, but may provide up to 50% of the equivalent dose; (c) the biological effects of HZE particles are not yet known and experimental ground-based experiments are needed for several biological endpoints (Durante et al., 2001) (see for example the experiments carried on in Brookhaven with iron ions); (d) radiobiological models and simulations based on a mechanistic description of biological damage need further developments to reliably predict the effects of mixed fields. In all of these cases the contribution of Monte Carlo transport codes is crucial.

The best way to describe the radiation field is undoubtedly to use fluencies. This is particularly true when one wants to understand radiation damage mechanisms. It is well known that LET is a "weak" quantity for predicting radiation effects. Even α particles and protons of the same LET can have different radiobiological effectiveness, due to the different velocities that determine different ionization clustering properties (Ottolenghi et al., 1997, 2001). Things are even more complicated with heavy ions, for which the same particle type with the same LET may have different biological effectiveness, again depending on their velocity. Nevertheless the LET and its various types of average values (typically track- and dose-average LET) and distributions are still frequently used to provide a first-approximation synthetic description of the radiation quality. Moreover, the LET is still used as a reference quantity to determine the quality factors when weighting factors are not defined in radiation protection (ICRP, 1991). In any case the use of track-average LET (and its corresponding microdosimetric quantity Y_F) is of scarce usefulness since it gives an unreasonable emphasis to the role of the flux of low-LET particles, which are of minor importance both in terms of dose and in terms of biological effectiveness. Moreover, in this work we will also show the large uncertainty (and the large dependence on experimental conditions and assumptions) in the determination of its values. If one has to use an average value we suggest to use the dose-average LET (and its corresponding microdosimetric quantity Y_D) which has a more soundly based justification both in terms of its predictive ability and in terms of theoretical and experimental determinations.

In this context, benchmark studies on LET distributions and average values, involving both theoretical models (and simulation codes) and experimental measurements, have become crucial particularly for iron ions, extensively used in radiobiological experiments. In this paper, the application of the FLUKA simulation code to ion beam studies is presented and discussed.

FLUKA (Fassò et al., 2001a; Fassò et al., 2001b) is a transport and interaction Monte Carlo code, capable of handling hadronic and electromagnetic showers from thermal neutrons up to very high energies (10,000 TeV). Being based, as far as possible, on well tested microscopic models, it ensures a high level of accuracy and versatility, it preserves correlations within interactions and among the shower components, and it provides predictions where no experimental data is directly available. When needed, powerful biasing techniques are available to reduce computing time. Descriptions of FLUKA models and extensive benchmarking can be found in the literature (Fassò et al., 2001a; Fassò et al., 2001b; http://www.fluka.org).

In the recent years, FLUKA has been successfully extended (Andersen et al., 2004) to nucleus–nucleus collisions. The DPMJET (Ranft, 1995; Roesler et al., 2001) code has been interfaced to cover the high (>5 GeV/n) energy range, and an extensively modified version of the RQMD-2.4 code (Sorge et al., 1989a,b; Sorge, 1995) is used at lower energies.

2. Ion–ion interactions in FLUKA

DPMJET (Ranft, 1995), a Monte Carlo model for sampling hadron–hadron, hadron–nucleus and nucleus–nucleus collisions at accelerator and cosmic ray energies, was adapted and interfaced to the FLUKA program. The original interface to the DPMJET-II.53 version has recently been upgraded to comply with the DPMJET-III version. DPMJET is based on the two component Dual Parton Model in connection with the Glauber formalism. FLUKA implements DPMJET as event generator to simulate nucleus–nucleus interactions exclusively. De-excitation and evaporation of the excited residual nuclei is performed by calling the FLUKA evaporation module.

The RQMD-2.4 (Sorge et al., 1989a; Sorge, 1995) is a relativistic QMD model which has been applied successfully to relativistic AA particle production over a wide energy range, from ≈0.1 GeV/n up to several hundreds of GeV/n. A RQMD-2.4 interface was developed to enable FLUKA to treat ion interactions from ≈100 MeV/n up to 5 GeV/n where DPMJET starts to be applicable. Several important modifications have been implemented in the RQMD code, in order to ensure energy-momentum conservation taking into account experimental binding

energies, and to provide meaningful excitation energies for the residual fragments. The results of this modified model in the energy range of interest for the applications described here can be found in Andersen et al. (2004) and Fassò et al. (2003).

Coulomb excitation of a target nucleus by the electromagnetic field of the projectile cannot be neglected in certain cases. It gets important at high energies and results in electromagnetic dissociation (ED) of the projectile nucleus. An ED model has recently been implemented in FLUKA, based on the standard approach for the calculation of the cross and on elementary photon–nucleon and photo-nuclear cross-sections stored in the program database.

3. Fragmentation of therapeutic ion beams

Fragmentation of therapeutic ion beams results in the attenuation of the impinging projectiles and the yield of secondary particles which can considerably influence the pattern of the dose delivery and the biological effectiveness of the irradiation. It is often regarded as an undesirable drawback which deteriorates the selective energy deposition due to the more frequent electromagnetic energy losses. However, the production of a minor amount of positron emitting fragments (from target, and, for ions with $Z \geqslant 5$, also from projectile) offers the possibility to monitor in situ and non-invasively the precision of the treatment by means of positron-emission-tomography (PET) (Enghardt et al., 1992). The induced β^+-activity distribution is correlated but not proportional to the applied dose. Hence, a reliable description of positron emitter production in the patient is necessary in order to extract valuable clinical information from the comparison with the measurement (Enghardt et al., 2004). FLUKA has been proved to be a suitable tool for this purpose in the case of proton beams (Parodi et al., 2002). Furthermore, it enables a realistic description of the tissue stoichiometry (Fiedler et al., 2004), which has been experimentally demonstrated to be an important issue for light ions (Parodi et al., 2004). Therefore, the extensibility of FLUKA to heavier projectiles is currently under investigation in view of its clinical application to PET monitoring at future facilities delivering a wide spectrum of ion beams from protons up to oxygen nuclei like at the Heavy Ion Cancer Therapy (HICAT) facility under construction in Heidelberg, Germany (Eickhoff et al., 2003). As a prerequisite for a correct prediction of positron emitter production, the fluence of primary and secondary particles has to be accurately reproduced by the code. For validation, fragmentation of therapeutic ion beams in tissue-like material was studied in comparison to experimental data from Schall et al. (1996) and Schall (1994). In this experiment, fluence distributions of primary ions and projectile fragments of a given charge Z were measured by detecting the escaping particles from an adjustable water absorber (0–25.5 cm) bombarded by ^{12}C, ^{14}N and ^{16}O beams at about 670 AMeV initial energy.

In the simulation, the corresponding particle fluences were scored in 1 mm thick slices perpendicular to the beam in a 30 cm long water phantom. Upstream beam elements could not be modelled in the simulation due to lack of detailed information. Only an approximate correction accounting for the loss of primary ions, energy degradation, and initial fragmentation at zero penetration depth was applied. Preliminary results show a fairly good agreement with the measured attenuation of the primary beam and the build-up of projectile fragments of $Z > 4$, as depicted in Figs. 1 and 2. Minor discrepancies observed in the oxygen case are consistent with a slight underestimation of proton emission with respect to neutron emission, that demands further investigations. The study of lower Z ($\leqslant 4$) fragments required a more realistic modeling of the setup due to their broader angular distribution and the limited acceptance of the detector. Moreover, the separate contribution of these light fragments could not be resolved in the measurements of Schall et al. (1996) and Schall (1994). Hence, the production and angular distribution of light charged particles ($Z \leqslant 2$) was validated further in comparison to more recent measurements performed at GSI Dartmstadt. The promising results of these latter studies in combination with analysis of total and partial charge changing cross-sections against additional experimental data from the literature will be reported soon in a separate contribution.

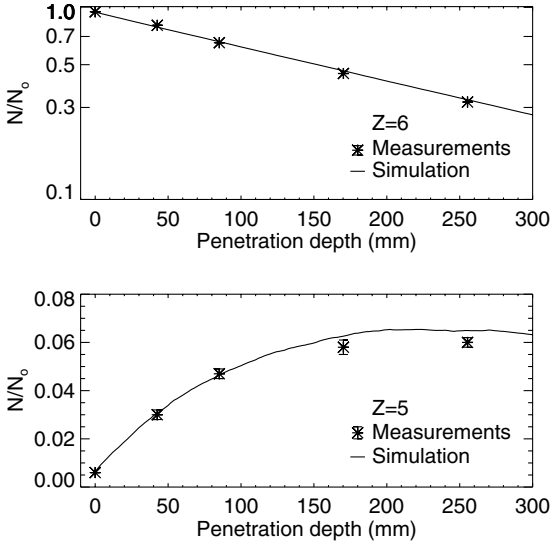

Fig. 1. 676 AMeV ^{12}C beam on a water phantom. Top: Carbon ion intensity as a function of depth. Bottom: Build-up of boron ions as a function of depth. Experimental data from Schall et al. (1996) and Schall (1994).

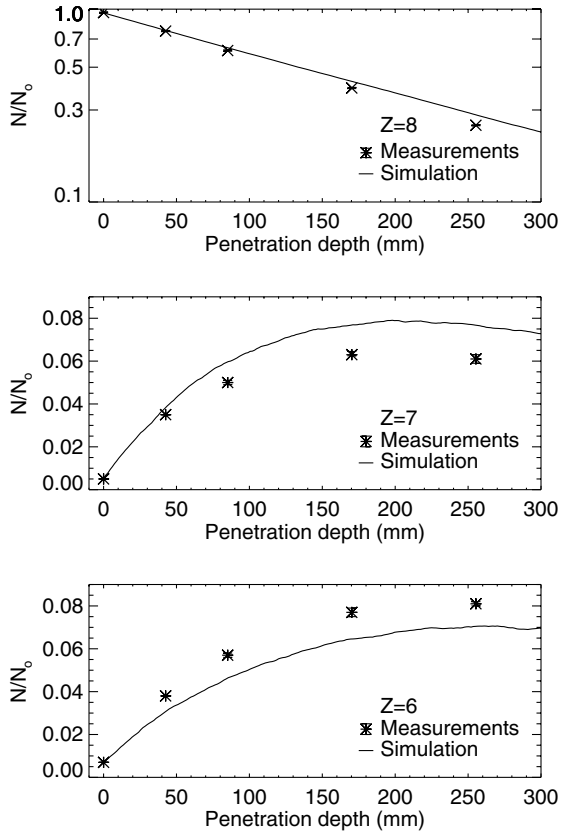

Fig. 2. Simulation of a 672 AMeV ^{16}O beam on a water phantom in comparison to experimental data from Schall et al. (1996) and Schall (1994): oxygen ion intensity (top), build-up of nitrogen (middle) and carbon ions (bottom) as a function of depth.

4. 1 GeV/n Fe ions

Although the goal of this exercise was to cross-check different calculations and compare them with experimental data, it allowed us to investigate the significance of dosimetric quantities and the influence of beam parameters on the results.

The basic simulation setup modeled an ideal case, that is an infinite uniform and parallel 1 GeV/n Fe beam, propagating through laterally "infinite" PMMA, (polymethyl metacrylate, density $\rho = 1.2$ g/cm^3) aluminum, and lead targets. This setup allows us to study the evolution of energy deposition and fragment spectra as a function of depth, and to investigate the dependence of the results on the angular acceptance and energy threshold. The same exercise has been repeated with different beam geometries and energy distributions. In addition to this, "real" cases have also been modeled: finite layers of PMMA (23 g/cm^2), and Al (7 g/cm^2) followed by silicon detector telescopes.

The analysis of simulated quantities allowed us to obtain:

- Fragment spectra.
- Energy deposition (dose).
- LET-derived dose $D_L = \int dL \cdot L \int d\Omega \cdot n(L,\theta)/\cos(\theta)$.
- Track-average LET $L_T = \int dL \cdot L \cdot f(L)$.
- Dose-average LET $L_D = \int dL \cdot L^2 \cdot f(L)/L_T$.

where $n(L,\theta) \cdot dL \cdot d\Omega$ is the number of incident particles per unit area with LET L and incident angle θ, and $f(L) \cdot dL$ is the relative frequency of particles with LET L. In the "ideal" cases, all quantities have been determined as a function of the depth inside the target. For the "real" cases with finite thickness, the information has been derived only at the target exit, from energy deposition spectra in the downstream silicon detectors.

4.1. 1 GeV/n Fe "perfect beam": dose and fragment spectra

Dose in the different materials has been calculated at different depths, both as true energy deposition and as derived from the charged particle LET. The LET-derived dose was also calculated considering only tracks whose direction with the original beam direction was within a 3° cone, to mimic the response of a hypothetic downstream detector with 3° angular acceptance. Values have been transformed to dose in water by scaling with the ratio of stopping powers at the nominal beam energy. The fragment charge distribution has also been recorded at the same positions, with and without angular cuts. Results are shown in Figs. 3–6. Dose values are normalized to unit beam fluence, spectra to one primary ion. There is clear agreement between the dose from energy deposition and the dose from LET with no angular cuts. The 3° restriction leads to a lower calculated dose (around 10–20% discrepancy). The discarded contributions come mainly from electrons/positrons and low Z fragments, as demonstrated for example by the plot in the right panel of Fig. 6. There, a further distinction has been made between the total charged particle distribution and the one restricted to nuclear fragments only. (i.e. with the exclusion of electrons, positrons and pions). Fig. 6 shows that electrons contribute substantially to the particle flux, and that particles up to $Z = 2$ are severely underestimated when an angular cut is applied (the same considerations are valid for the other materials/depths).

4.2. 1 GeV/n Fe beam parameters

The effect of small variations in the beam parameters are shown in Fig. 7. The following cases have been considered:

- parallel beam with fixed 1 GeV/n energy (basic case),
- parallel beam 1 GeV/n with 2 MeV/n FWHM energy spread,
- parallel beam 1.05 GeV/n with 2 MeV/n FWHM energy spread,

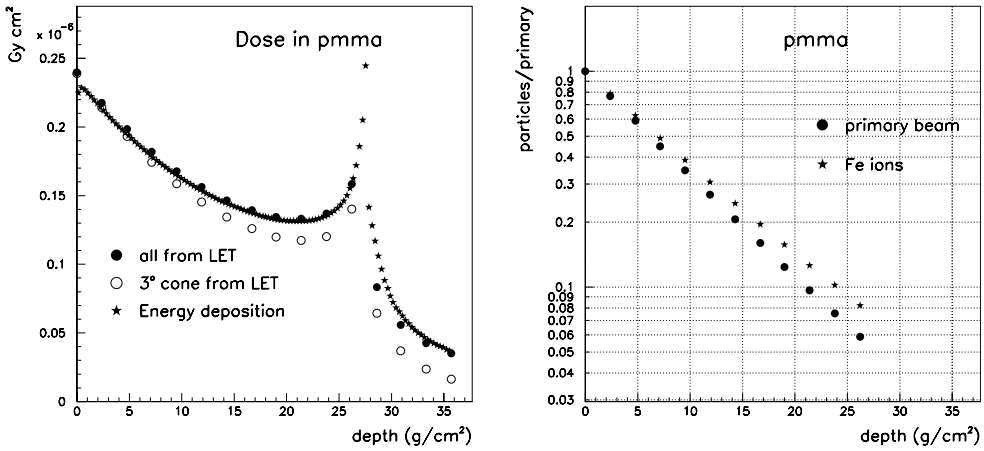

Fig. 3. Left: absorbed dose as a function of depth in PMMA ("true" and as derived from the charged particle LET); Right: uncollided ("primary") and $Z = 26$ ion survival in PMMA.

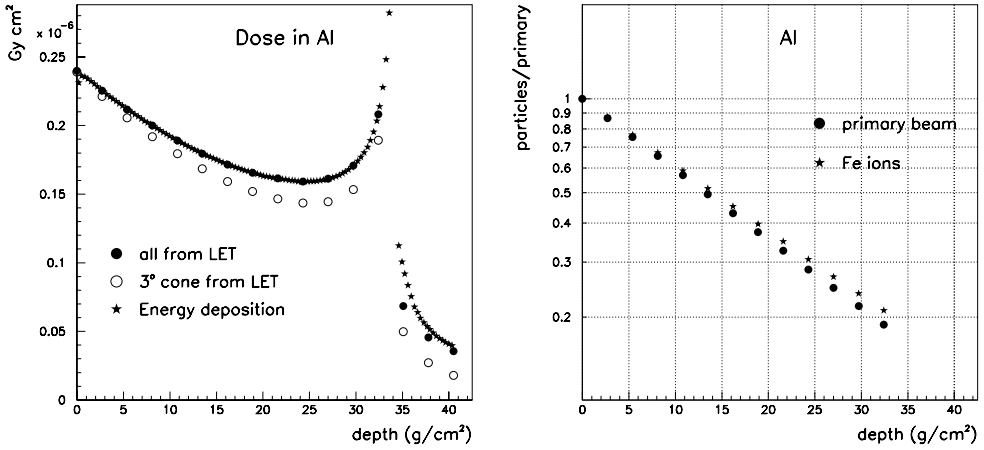

Fig. 4. Left: absorbed dose as a function of depth in aluminum ("true" × 1.26 and as derived from the charged particle LET); Right: uncollided ("primary") and $Z = 26$ ion survival in aluminum.

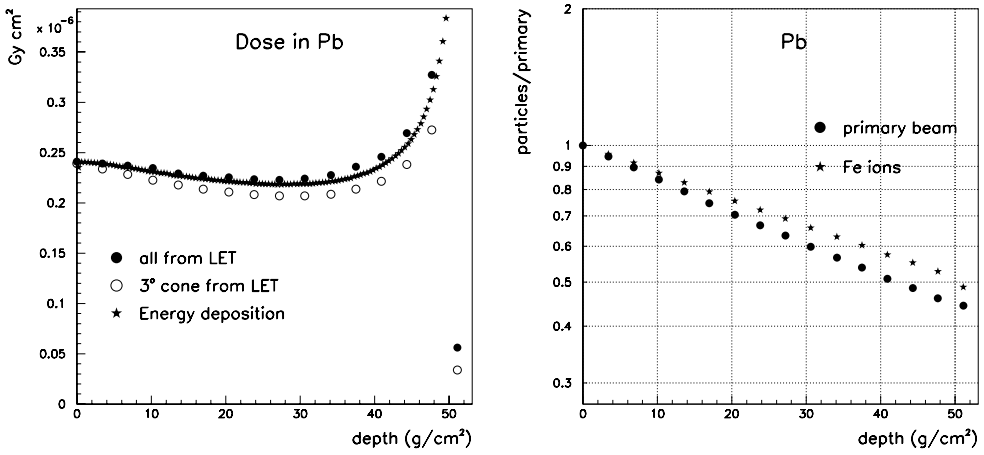

Fig. 5. Left: absorbed dose as a function of depth in lead ("true" × 1.86 and as derived from the charged particle LET); Right: uncollided ("primary") and $Z = 26$ ion survival in lead.

- 1 GeV/n beam with 2 MeV/n FWHM, 5 mrad divergence, 7 cm radius and intensity 85% at $R = 7$ cm (label "real" in the plot). In this case, dose was evaluated within a 1 cm radius around the beam axis.

There is substantial agreement of results among the ideal case, the "real" case and the energy spread case at 1 AGeV. Conversely, a 5% increase in the beam energy moves the Bragg peak position of almost 10%,

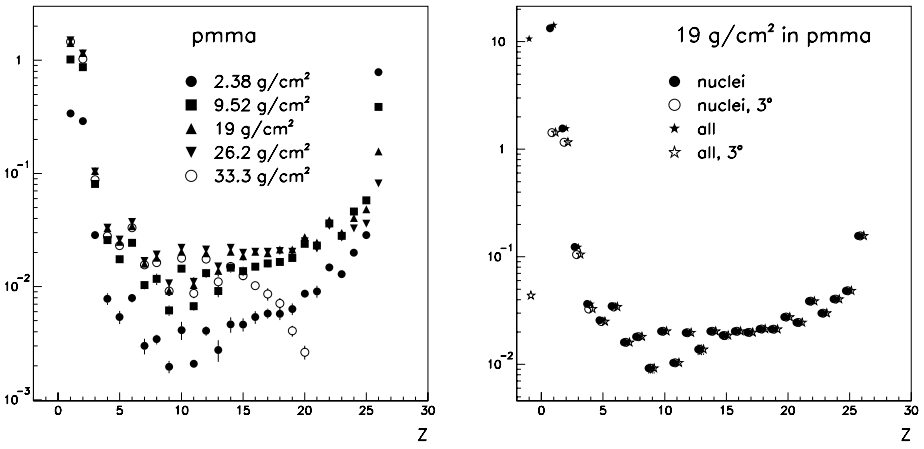

Fig. 6. Left: fragment spectra as a function of depth in PMMA (nuclei only, 3° cone) Right: fragment spectra at 19 g/cm^2 in PMMA for all charged, nuclei only, and with or without a 3° cut.

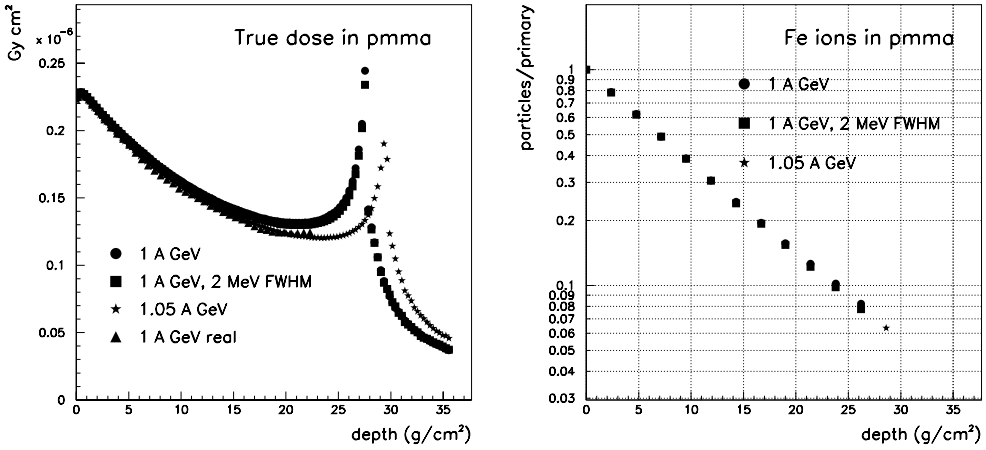

Fig. 7. Left: absorbed dose as a function of depth in PMMA for Fe beams having different beam parameters (see text for details) Right: $Z = 26$ ion survival in PMMA for parallel Fe beams around 1 GeV/n.

and gives ≈25% lower peak dose, due to the beam attenuation by nuclear interactions, that scales exponentially with the traveled distance (Fig. 7, right panel).

4.3. LET in "ideal" case

Track-average and dose-average LET have been calculated as a function of depth for the ideal beam case, in the different materials under consideration. In order to understand what are the possible distortions induced by experimental effects, several cuts/conditions have been examined:

- the "true" quantity from all charged particles;
- considering only nuclear fragments;
- considering only nuclear fragments within a 3° cone;
- from all charged particles, with a threshold on the LET value that discards the signal due to electrons;
- as above, adding the 3° angular cut.

The LET threshold cut simulates the experimental condition where the electron signal cannot be distinguished from pedestal. Results are shown in Fig. 8 for an Al layer. The behavior is similar for the other materials under consideration. The track average LET shows a dramatic dependence on the "experimental" details. In particular, the effect of a threshold on the LET increases the average of an order of magnitude with respect to the "true" one, and introduces an unphysical dependence on depth. The effect of threshold is higher than the effect of discarding only electrons (case "nuclei") because relativistic light fragments (protons) have LET or Si energy deposition values which somewhat overlap with those of electrons. The angular acceptance enhances this effect, as already discussed in relation to the fragment charge distributions. The dose average LET shows on the contrary a stable behavior, with a longitudinal profile similar to the dose profile.

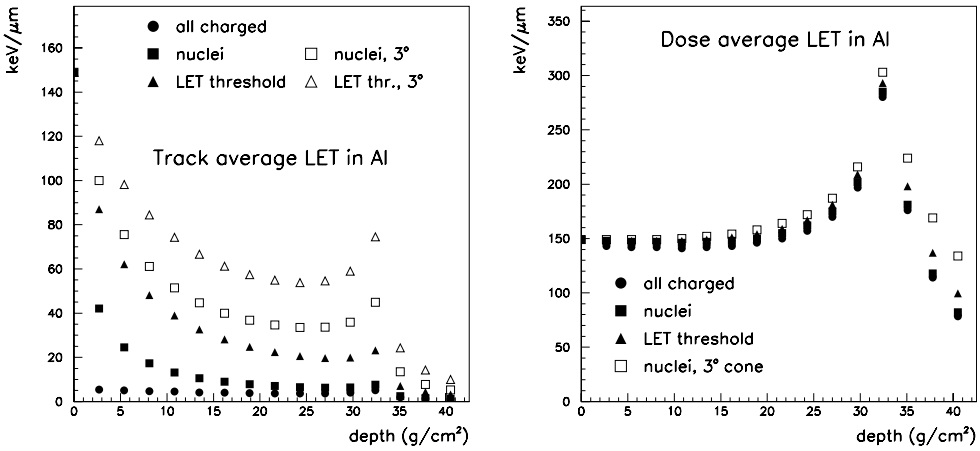

Fig. 8. Left: track-average LET as a function of depth. Right: dose-average LET as a function of depth. Both for a parallel monochromatic Fe ion beam of 1 GeV/n in aluminum.

4.4. Finite geometry and silicon telescopes

Two cases with real targets and detectors have been simulated:

- 7.02 gm/cm^2 aluminum target, with 4 silicon detectors disposed in two pairs, 5 mm thickness and 2 cm active radius at distances of 110.5, 112.5, 155 and 157 cm from the center of the target.
- 22 gm/cm^2 PMMA target, with 4 silicon detectors, 3 mm thickness and 1.2 cm active radius at 20.3, 22.3, 61 and 63 cm distance.

The simulated setup is a schematic representation of the Brookhaven experimental apparatus, following the specifications from Miller (2004). The targets were hit by 1 AGeV broad iron ion beam (7 cm radius like in the previous section). Tests have also been performed with a pencil beam. Charged particle spectra, track average LET and dose average LET have been derived from simulated data. Since background rejection is normally performed in experimental data with cuts on the correlations among detectors, several cut conditions have also been applied to simulated data. Charged particle spectra have been inferred from energy deposition spectra, considering the summed signal of one pair of detectors and assuming that the signal is proportional to the square of the charge, the highest peak giving the calibration: $Z_{\mathrm{eff}} = 26 \times \sqrt{\Delta E/\Delta E_{\mathrm{peak}}}$ where ΔE is the energy deposited in the detectors. The signal has been accepted only if the signals in the two detectors are consistent within ±30%, that is a crude approximation of the experimental cuts.

While well defined peaks are present in the thin target case, the charge spectrum for thick targets does not allow to really distinguish the fragment charge. The hypothesis of constant velocity, on which the reconstruction is based, clearly fails if the amount of traversed material is not negligible, and the probability to have multi-particle events is substantial.

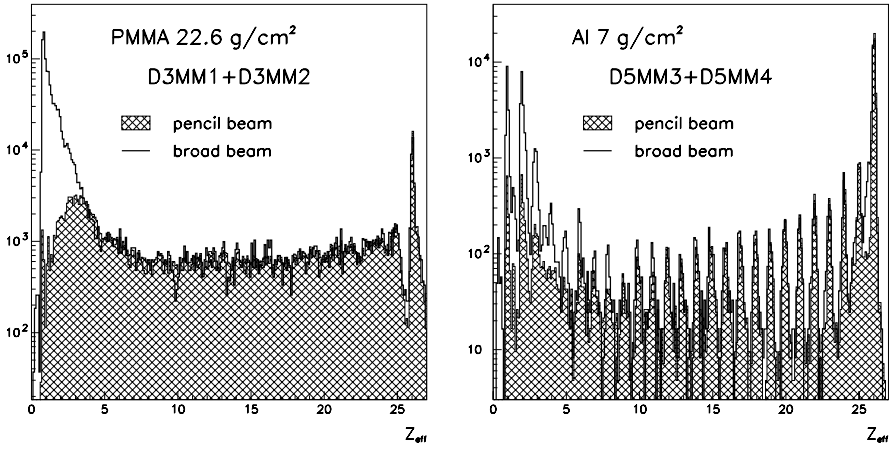

Fig. 9. Z_{eff} for PMMA (23 g/cm^2, left) and Al (7 g/cm^2, right) (see text for details). Calculations for nominal (R = 7 cm) and pencil beams are shown, normalized to the same Z = 26 peak integral.

Table 1
Various estimations of track-average LET and dose-average LET at silicon detector level for the 23 g/cm^2 case (*Note that the beam is 1 GeV/n, not 1.05!!*)

Det.	Track-average LET (keV/μm)							Dose-average LET (keV/μm)						
	$\mathscr{A}$	$\mathscr{B}$	$\mathscr{C}$	$\mathscr{D}$	$\mathscr{E}$	$\mathscr{F}$	$\mathscr{G}$	$\mathscr{A}$	$\mathscr{B}$	$\mathscr{C}$	$\mathscr{D}$	$\mathscr{E}$	$\mathscr{F}$	$\mathscr{G}$
1	5.1	6.6	29	51	45	114	17	161	162	171	178	174	173	163
2	5.3	6.9	30	51	47	118	17	167	169	178	184	182	180	170
3	9.8	12	31	58	45	127	13	177	178	188	195	190	188	163
4	8.8	13	31	61	47	132	13	186	187	199	208	202	199	175

A strong suppression of the low-Z fragments in the pencil beam case with respect to the the broad beam case is observed (see Fig. 9), in analogy with the angular cut effect described in the previous paragraphs.

Track average LET and dose average LET have been calculated from each of the detectors separately, with cuts on the signal correlation in a detector pair or among all detectors. Since the silicon detectors have no segmentation, and therefore no capability to separate different tracks, the track average LET is indeed poorly defined, being obtained as it came from a single track even in the case of high multiplicity. This has clearly the effect of a huge increase of its value above the true one, and above the one that could be obtained with a segmented detector. Results of the simulations for the PMMA target are summarized in Table 1, for the following cases:

- $\mathscr{A}$ "True", from all particle counting.
- $\mathscr{B}$ From nuclei only particle counting.
- $\mathscr{C}$ From Si energy deposition, asking a loose consistency condition: signal within 1/5 and 5 times the four-detectors average.
- $\mathscr{D}$ From Si energy deposition, asking for a signal within 30% from the four-detectors average.
- $\mathscr{E}$ From Si energy deposition, with a 30% consistency between detectors in a pair.
- $\mathscr{F}$ From Si energy deposition, with contour cut in the correlation plot of a Si pair, similar to La Tessa (2004).
- $\mathscr{G}$ Like $\mathscr{E}$, but assuming the detector has a 100 fold "pixel-like" granularity.

5. Conclusions

Simulation of ion transport and interaction is the present main FLUKA development area. New features include the upgrade of the DPMJET interface to DPMJET-III, and the development of an electromagnetic dissociation model. Comparison of the code results with experimental data assess the code reliability and provide a sound basis for the application in many different fields. The encouraging results of an application to therapy beams have been described. The FLUKA capability to describe microscopically all physical processes in full three-dimensional geometry, reproducing internal correlations among reaction products and treating in a single run all shower components, allow to investigate beam and experimental effects on commonly derived/measured quantities. This has been performed here for 1 AGeV Fe ions in various targets, in "ideal" and "real" conditions. A few conclusions can be outlined:

- The relative contribution of light ions shows up to be sensitive to beam, target and detector geometry.
- Results from medium/thick targets are dominated by energy spread and showering in the target, therefore giving little insight on the basic processes.
- Track average LET estimations appear hopelessly sensitive to experimental conditions/thresholds, and its uncertainty further support its uselessness for heavy-ion radiobiological studies.

Acknowledgments

This work was partially supported under: NASA Grants: NAG8-1658 and NAG8-1901, DOE contract DE-AC02-76SF00515, ASI Contract I/R/320/02, European Union contract no. FI6R-CT-2003-508842, "RISC-RAD".

References

Andersen, V., Ballarini, F., Battistoni, G., et al. The FLUKA code for space applications: recent developments. Adv. Space Res. 34, 1302–1310, 2004.

Durante, M., Antonelli, F., Ballarini, F., et al. Space radiation shielding: biological effects of accelerated iron ions and their modification by aluminum or lucite shields. Micrograv. Space Stat. Utiliz. 2, 179–181, 2001.

Eickhoff, H., Bär, R., Dolinskii, A., et al. HICAT-The German Hospital-Based Light Ion Cancer Therapy Project, in: Chew, J., Lucas, P., Webber, S. (Eds), Proceedings of the 2003 Particle Accelerator Conference (PAC), 12–16 May, Portland, OR, pp. 694–698, 2003.

Enghardt, W., Fromm, W.D., Geissel, H., et al. The spatial distribution of positron-emitting nuclei generated by relativistic light ion beams in organic matter. Phys. Med. Biol. 37, 2127–2131, 1992.

Enghardt, W., Crespo, P., Fiedler, F., et al. Charged hadron tumour therapy monitoring by means of PET. Nucl. Instr. Meth. A 525, 284–288, 2004.

Fassò, A., Ferrari, A., Sala, P.R. FLUKA: status and prospective for hadronic applications. In: Kling, A., Barão, F., Nakagawa, F., et al. (Eds.), Proceedings of the MonteCarlo 2000 Conference. Springer Verlag, Berlin, pp. 955–960, 2001a.

Fassò, A., Ferrari, A., Sala, P.R. Electron–photon transport in FLUKA: status. In: Kling, A., Barão, F., Nakagawa, F., et al. (Eds.), Proceedings of the MonteCarlo 2000 Conference. Springer Verlag, Berlin, pp. 159–164, 2001b.

Fassò, A., Ferrari, A., Roesler, S., et al. The physics models of FLUKA: Status and recent development, eConf C0303241, MOMT005, 2003.

Fiedler, F., Parodi, K., Ferrari, A., Enghardt, W. The prediction of the β^+-activity distribution on the basis of the treatment planning CT using the FLUKA simulation code. Forschungszentrum Rossendorf Wiss.-Tech. Ber. FZR-401, 69, 2004.

ICRP 1990 Recommendations of the International Commission on Radiological Protection, ICRP Publication 60, Annals of the ICRP, vol. 21, N 1–3, Pergamon Press, Oxford, 1991.

La Tessa, C., paper F2.3-0009-04, presented at this conference.

Miller, J., private communication.

Ottolenghi, A., Merzagora, M., Paretzke, H.G. DNA complex lesions induced by protons and alpha particles: track structure characteristics determining LET and particle type dependence. Radiat. Environ. Biophysics, Berlin, Germany 36, 97–103, 1997.

Ottolenghi, A., Ballarini, F., Biaggi, F. Mechanistic and phenomenological models for the estimate of radiation-induced biological damage. Phys. Med. 17, 3–12, 2001.

Parodi, K., Enghardt, W., Haberer, T. In-beam PET measurements of β^+-radioactivity induced by proton beams, Phys. Med. Biol. 47, 21–36, 2002.

Parodi, K., Pönisch, F., Enghardt, W. Experimental investigations on in-beam PET for proton therapy. Forschungszentrum Rossendorf Wiss.-Tech. Ber. FZR-401, 66, 2004.

Ranft, J. Dual parton model at cosmic ray energies. Phys. Rev. D51, 64–84, 1995.

Roesler, S., Engel, R., Ranft, J. The Monte Carlo event generator DPMJET-III, in: Proceedings of the MonteCarlo 2000 Conference, Lisbon, 23–26 October 2000, Springer Verlag Berlin, pp. 1033–1038, 2001.

Schall, I. Ph.D. Thesis, Technische Hochschule Darmstadt, 1994.

Schall, I., Schardt, D., Geissel, H., et al. Charge-changing nuclear reactions of relativistic light-ion beams ($5 \leqslant Z \leqslant 10$) passing through thick absorbers. Nucl. Instr. Meth. B 117, 221–234, 1996.

Sorge, H., Stöcker, H., Greiner, W. Relativistic quantum molecular dynamics approach to nuclear collisions at ultrarelativistic energies. Nucl. Phys. A 498, 567–576, 1989a.

Sorge, H., Stöcker, H., Greiner, W. Poincaré invariant Hamiltonian dynamics: Modelling multi-hadronic interactions in a phase space approach. Ann. Phys. N.Y. 192, 266–306, 1989b.

Sorge, H. Flavor production in Pb(160 AGeV) on Pb collisions: Effect of color ropes and hadronic rescattering. Phys. Rev. C52, 3291–3314, 1995.